JGR Biogeosciences

RESEARCH ARTICLE
10.1029/2018JG004640

Key Points:
- We propose a probabilistic model where we determine changes in the exceedance probability of soil respiration due to changes in variables
- Soil respiration (CO_2 flux) follows a Gaussian-like (bell-shape) pattern with increasing soil temperature
- When temperature exceeds the dew point, soil respiration has the potential to raise up to 60% higher compared to dry condition

Correspondence to:
H. Anjileli,
hassan.a@uci.edu

Citation:
Anjileli, H., Moftakhari, H. R., Mazdiyasni, O., Norouzi, H., Ashraf, S., Farahmand, A., et al. (2019). Analyzing high-frequency soil respiration using a probabilistic model in a semiarid, Mediterranean climate. *Journal of Geophysical Research: Biogeosciences*, *124*, 509–520. https://doi.org/10.1029/2018JG004640

Received 5 JUN 2018
Accepted 31 JAN 2019
Accepted article online 4 FEB 2019
Published online 5 MAR 2019

Analyzing High-Frequency Soil Respiration Using a Probabilistic Model in a Semiarid, Mediterranean Climate

H. Anjileli[1], H. R. Moftakhari[1,2], O. Mazdiyasni[1], H. Norouzi[3], S. Ashraf[1], A. Farahmand[4], P. Bowler[5], M. Azarderakhsh[6], Travis E. Huxman[5], and A. AghaKouchak[1,7]

[1]Department of Civil and Environmental Engineering, University of California, Irvine, CA, USA, [2]Civil, Construction and Environmental Engineering, University of Alabama, Tuscaloosa, AL, USA, [3]Department of Construction Management and Civil Engineering, New York City College of Technology, The City University of NY, Brooklyn, NY, USA, [4]NASA Jet Propulsion Laboratory, California Institute of Technology, Pasadena, CA, USA, [5]Department of Ecology and Evolutionary Biology, University of California, Irvine, CA, USA, [6]School of Engineering and Computer Sciences, Fairleigh Dickinson University, Teaneck, NJ, USA, [7]Department of Earth System Science, University of California, Irvine, CA, USA

Abstract High-frequency (subhourly) changes in soil respiration (*Rs*), a critical component of the carbon cycle, are not well documented in semiarid ecosystems. We investigate the response of *Rs* to subhourly soil temperature (*T*soil) and soil volumetric water content (VWC) variation in a semiarid ecosystem across a year of highly variable weather. We propose a probabilistic model to estimate the likelihood of *Rs* exceeding its annual mean (1.2 μmol CO_2/m^2s), conditioned on different *T*soil and VWC values. The results show that *Rs* follows a Gaussian-like pattern as *T*soil increases, where it follows an upward trend until ~18 °C, and then begins to decline. *Rs* remains constant at *T*soil beyond ~27 °C. Using our novel conditional probability model, we show both the increasing and decreasing response of *Rs* to rising *T*soil through two ranges (14–17 and 20–23 °C) where *Rs* observations show opposing responses. We demonstrate that an increase in *T*soil from 14 to 17 °C causes a rise in *Rs* by a factor of 1.4 relative to the mean. The proposed model also describes how *Rs* reduces as *T*soil continues to increase above ~18 °C. Considering VWC and *T*soil into the proposed model, we show that when *T*soil is low (e.g., 17 °C), a rise in VWC yields a decrease of *Rs* by a factor of 3.6. However, when *T*soil is high (e.g., 23 °C), *Rs* increases with increasing VWC by a factor of 2.5. Overall, the probabilistic model enables us to detect and characterize changes in *Rs* distribution in response to different environmental variables and thresholds.

1. Introduction

Carbon cycling in semiarid areas may be particularly sensitive to global climate change (Huang et al., 2016) given the ecological and evolutionary dynamics of plants and microbes associated with episodic rainfall input (Huxman et al., 2004) and the magnitude of change in key drivers for these regions of the globe (Weltzin et al., 2003). Carbon dioxide (CO_2) flux from the soil to the atmosphere, also referred to as soil respiration, is a critical component of the carbon cycle (Cable et al., 2011). Soil respiration (*Rs*) is the second major contributor to the global CO_2 flux and is indeed around 9 times larger than the anthropogenic CO_2 emissions (Carey et al., 2016; Giardina et al., 2014; Raich & Schlesinger, 1992). *Rs* is associated with the metabolic activity of organisms found in the soil, typically deconstructed as heterotrophs (e.g., decomposing microbes) and autotrophs (e.g., roots and associated symbiotic microbes; Cable et al., 2008). Terrain level, vertical depth of soil, spatial characteristics of the local site, and soil and vegetation type all play roles in the rate of respiration (Cannone et al., 2012; Janssens et al., 2001; Maier et al., 2011). However, the primary abiotic factors controlling the pattern and magnitude of *Rs* are soil temperature (*T*soil) and soil volumetric water content (VWC; Liang et al., 2017; Ryan & Law, 2005).

The estimated quantity of carbon stored in and emitted from soil including peatlands, wetlands and permafrost, has been recently studied (Davidson & Janssens, 2006; Scharlemann et al., 2014). However, a significant lack of knowledge exists about the distribution of carbon and *Rs* of soil in semiarid ecosystem (Schimel, 2010) and the way these variables respond to climate change (Graf Pannatier et al., 2012; Zhong et al., 2016). Thus, any small changes in the underground carbon pools might have large impacts on carbon flux into the atmosphere (Fabianek et al., 2015; Hirano, 2003; Ryan & Law, 2005).

Several methods have been employed to study the changes of *Rs* due to climate variability, through field/laboratory experiments (e.g., soil warming; Carey et al., 2016; Hicks Pries et al., 2017; Schindlbacher et al., 2012), models (e.g., Century, Rothamsted Carbon Model [RothC], Earth System Model [ESMs] from Coupled Model Intercomparison Project Phase 5 [CMIP5]) (Lehmann & Kleber, 2015; Todd-Brown et al., 2013; Wieder et al., 2013), and biosphere-atmosphere exchange (e.g., Fluxnet; Phillips et al., 2017), by using deterministic models. These studies provide crucial information about changes of *Rs* (e.g., standard deviation, mean, and range). However, hardly any endeavor has been made to describe the change in the entire probability distribution of *Rs* under different hydroclimatic conditions. Such approach provides new insights in detecting changes in the *Rs* distribution in response to shifts in drivers (i.e., determining changes in the exceedance probability [EP] of *Rs* due to changes in hydroclimatic variables).

Probabilistic models combined with high-frequency data set have been used in various fields and can reveal valuable information (e.g., analysis of extreme events, snowpack response to warming, nuisance flooding, and compounding effects; e.g., Cheng et al., 2014; Huning & AghaKouchak, 2018; Mazdiyasni et al., 2017; Moftakhari et al., 2017; Papalexiou et al., 2018). The probability density functions (PDFs) used in this study show not only the most likely value (highest density) but also the entire distribution of the expected *Rs*. Furthermore, we can reflect the distribution of *Rs* conditioned on any hydroclimate variable of interest (e.g., *T*soil and/or VWC). The integral of the PDF above a given threshold (i.e., any threshold of interest) represents the EP of *Rs* (i.e., the likelihood that the designated threshold will be exceeded). By comparing two different exceedance probabilities, we can detect changes in the *Rs* distribution and therefore measure the impact on *Rs* given specific hydroclimate conditions. This means, probabilistic models not only provide a thorough insight of *Rs* dynamics but are also useful tools to characterize the impact of different hydroclimatic conditions on *Rs*. Using such models in conjunction with our measured subhourly high-frequency data set provides detailed, high-resolution probabilistic analysis on the impacts of hydroclimatic drivers on *Rs*.

The temperature sensitivity of *Rs*, described as the rate to which *Rs* increases or decreases in response to change in temperature, over a wide range of temperatures is not well understood in various biomes (e.g., forest, desert, and semiarid areas; Boone et al., 1998; Cable et al., 2011; Nuanez, 2015). From climate perspective, semiarid terrestrial ecosystems remain data poor, restricting our understanding of how *Rs* responds to *T*soil and VWC (Lellei-Kovács et al., 2011; Rey et al., 2011). This may stem from the fact that the *Rs* rate in semiarid ecosystems is the lowest in comparison with other biomes on Earth (Grünzweig et al., 2009; Oertel et al., 2016), and so their contribution to the total cycle is perceived to be relatively limited. This is not necessary true as arid/semiarid regions encompass one third of the global dryland (Williams, 1999), and so their contribution to the carbon cycle is significant (Schimel, 2010).

Regarding vegetation, *Rs* remains challenging on bare soil, due to its complicated biological and physical structure (Eugster & Merbold, 2015). In this perspective, we report subhourly measurements of *Rs* from bare soil in a semiarid Mediterranean ecosystem located in Southern California, which allows us to characterize pulse-driven dynamics at high frequencies (Evans & Wallenstein, 2012; Huxman et al., 2004; Jenerette et al., 2008). The goal of this study is to characterize the temporal variability of *Rs* under various hydroclimatic conditions. Using the probabilistic approach, we can assess the impacts of different temperatures and VWC ranges on *Rs*. In other words, we can more effectively detect the changes in the *Rs* distribution in response to shifts in drivers (e.g., determining changes in EP in response to increased *T*soil and decreased VWC). The objectives are (1) to quantify how *Rs* reacts to changes in *T*soil and VWC, (2) to describe the impacts of changes in *T*soil and VWC on the distribution of *Rs*, and finally (3) to investigate unexpected findings such as the role of dew on *Rs* in a semiarid area.

2. Materials and Methods

2.1. Site Description

The study area is located at the San Joaquin Marsh Reserve, adjacent to the University of California, Irvine. The San Joaquin Marsh Reserve is within the University of California Natural Reserve System, encompassing more than 817,500 m^2. It is subdivided into different sections, including man-made and untouched areas.

10.1029/2018JG004640

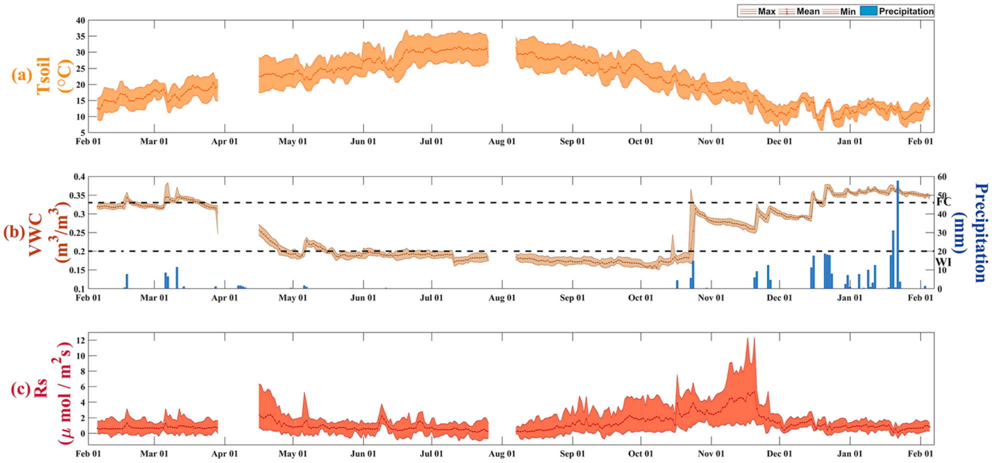

Figure 1. Daily meteorological parameters and *Rs* from February 2016 to February 2017. Max and min are displayed in solid lines and mean values are shown in dotted solid lines. *Rs* increases when precipitation happens. But higher precipitation does not always lead to higher *Rs* above a certain level of precipitation and *T*soil; *Rs* starts do decrease. This effect is shown in November and December. VWC = volumetric water content.

The measurement gauge is located in the untouched area (33° 39′32.7″N, 117° 50′55.9″W) at an elevation of 2 m above sea level. This region experiences a Mediterranean climate (i.e., mild, moderately wet winters and warm to hot, dry summers) with an average annual temperature of ~17 °C and a mean annual precipitation of 300 mm (Bowler, 2007). Investigated soils have been characterized as well drained omni clay with a pH of 8.5, calcium carbonate content of 3% (Bowler, 2007; California Resources Agency, 2007), and soil organic matter content of 3.5%. On average soil organic matter contains 58% carbon (van Bemmelen, 1891), we therefore presume a soil carbon content of 2%. The chemical property of the soil also shows calcium carbonate ($CaCO_3$) with an amount of 3% (Bowler, 2007; California Resources Agency, 2007; Web Soil Survey [WWW Document], n.d.). In addition, the soil based on the U.S. Department of Agriculture Natural Resources Conservation Service is classified as Omni with a taxonomic classification of fine, montmorillonitic (calcareous), and thermic Fluvaquentic Haplaquolls, Mollisols (Bowler, 2007; California Resources Agency, 2007; U.S. Department of Agriculture Natural Resources Conservation Service, n.d.). The moisture characteristics of the soil in terms of field capacity and wilting point for omni clay have been reported to be 0.33 and 0.20 m^3/m^3, respectively (Walker, 1989), which are shown as dashed lines in Figure 1b.

2.2. Soil Respiration and Additional Measurements

Soil respiration (*Rs*) was measured subhourly from February 2016 to February 2017 using an automated *Rs* system (LI-8100A, LI-COR, Inc., Lincoln, Nebraska, USA). The LI-8100A is an Automated Soil Gas Flux System, which measures CO_2 flux from the soil using a single long-term transparent chamber and an analyzer control unit (ACU). The infrared gas analyzer installed in the ACU measures the change in CO_2 in the chamber. One polyvinyl chloride collar with a diameter of 20.3 cm and height of 11 cm was inserted into the soil to a depth of 6 cm 1 week before measuring *Rs* to limit soil disturbance and to allow repeated measurements. The vegetation within the collar was cleared off to make sure that the soil remains bare over the entire observation period. The system was programmed to enable five measurements per hour with an observation period of 2 min. During each flux measurement, the chamber vented automatically for 65 s (45 s prepurge and 20 s postpurge). An umbrella was installed above the ACU to protect the analyzer from sunlight and to avoid overheating.

Simultaneously, soil temperature (*T*soil) and soil VWC near the chamber at 5-cm depth below ground surface were observed using an auxiliary soil temperature thermistor (LI-COR, Inc., Lincoln, NE, USA) and an ECH$_2$O model EC-5 (Decagon Devices, Inc., Pullman, WA, USA), respectively. Both sensors were attached to the LI-8100A ACU. The EC-5 determines the VWC by measuring the dielectric constant media using capacitance domain technology (Kočárek & Kodešová, 2012). The system was powered at the beginning of the observations with a 55-Ah/12 volt battery and a 60-W solar panel but upgraded to a 180 Ah/12 Volt battery with 260-W solar panels after several power failures. Due to the latest upgrade of the battery and solar panels, we limited the observations to five measurements per hour to ensure continuous day and night measurements. Approximately 7% of the *Rs* data were not captured due to instrument failure and insufficient power supply due to cloudy days.

To confirm the existence and effect of dew on *Rs*, we performed a short experiment of 2 days in mid-November. In this experiment we measured the soil surface temperature at the study site during night. Night surface soil temperature (*T*soil surface) inside the collar was obtained using an EasyLog EL-USB-2-LCD temperature data logger (Lascar Electronics Inc., Erie, PA, USA).

Daily meteorological data (e.g., dew point and precipitation) were obtained from the weather station at the John Wayne Airport (SNA), Santa Ana, CA (located within three kilometers from the study area), from the National Oceanic and Atmosphere Administration website (https://gis.ncdc.noaa.gov/maps/ncei/cdo/hourly).

2.3. Data Analysis

We use Spearman correlation coefficient (R^2) to evaluate the relationship between *Rs* and *T*soil and VWC due to existing time lags. These lags result in an elliptical hysteresis loop (Phillips et al., 2017; Song et al., 2015) and are caused, for instance, through the transport of *Rs* from various depth layers to the surface (Phillips et al., 2017), resulting in a delay in the *Rs* observation (Zhang et al., 2015). However, no guideline exists on how *Rs* data should be analyzed in order to determine the relationship between *Rs* and *T*soil (Phillips et al., 2011). We, therefore, use stepwise regression analysis through which we temporally adjust the time series of hydroclimatic parameters by stepwise shifting entire time series in time. Lag time-induced temporal adjustment of hydroclimate parameters and *Rs* continues till the vectors are synchronized based on the highest value of R^2. Our results show that, in the studied system, the lag time between *Rs* and hydroclimate parameters through the entire time series is ~6 hr. The stepwise regression technique used here reflects upon strong seasonality in *Rs* and thus varying lag times (Kuzyakov & Gavrichkova, 2010). The time lag between *Rs* and hydroclimate parameters for spring (20 March to 20 June), summer (21 June to 21 September), fall (22 September to 20 December), and winter (21 December to 19 March) season is estimated to be ~3, ~7, ~4, and ~10 hr, in the studied area, respectively. Henceforward, we use the adjusted time series in this research for further analysis.

To evaluate *Rs*-*T*soil and VWC-*T*soil relationships, we use the mean value of data points existing within a step size of 1 °C. We rank the *T*soil values from min to max and averaged all associated data points (e.g., *Rs* and VWC) within the given step size of 1 °C.

We quantify the temperature sensitivity of *Rs* (Δ*Rs*) and VWC (ΔVWC) using a moving average technique, which removes residuals and reveals the overall trend. By using moving bin average, we calculate the arithmetic mean of several consecutive values of different subsets from the whole data set. The temperature sensitivity (i.e., rate of change) is calculated through consecutive subtraction of the bin-averaged values at two consecutive calculating windows. The mathematical representation of the temperature sensitivity analysis process using moving bin-averaged technique is as follows:

$$\Delta = \frac{1}{x_2}\sum_{t=i+m}^{i+n+m} a_{t_2} - \frac{1}{x_1}\sum_{t=i}^{i+n} a_{t_1} \quad (1)$$

where n, m, i, $a_{t_{1,2}}$, and $x_{1,\ 2}$ represent length of moving average, step size, starting point, measured values (e.g., *Rs* and VWC) for *T*soil taking values of t, and number of data points, respectively. It is worth mentioning that the spans include different sample sizes. To calculate the Δ*Rs*, for example, we first rank the *T*soil values from min to max and then choose the starting point as the smallest observed *T*soil value (i.e., 5.5 °C). Then we calculate the mean of *Rs* measured within a span of 5 °C (e.g., T_8 refers to values associated within 5.5 to 10.5 °C) and a step size of 1 °C (e.g., T_9 would encompass the values associated within 6.5 to 11.5 °C). Finally, we subtract the bin-averaged values at the two consecutive bins ($T_{9\text{-}8}$).

10.1029/2018JG004640

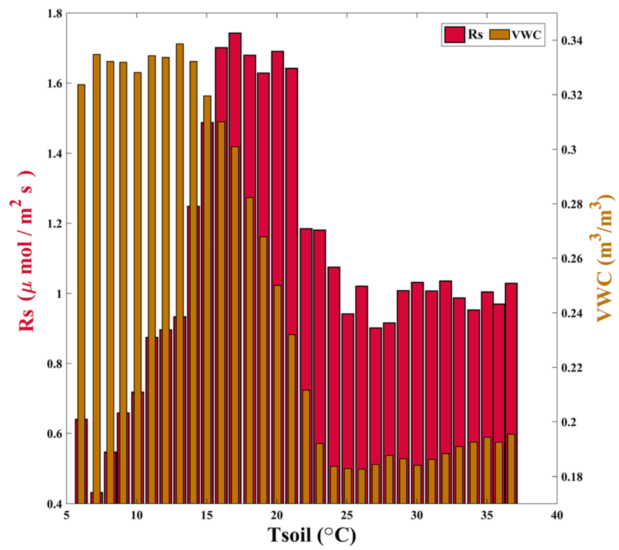

Figure 2. Hourly bin-averaged *Rs* and volumetric water content (VWC) across *T*soil ranges. *Rs* shows a Gaussian pattern and VWC displays a mirrored sigmoid pattern. *Rs* increases until ~18 °C with increasing *T*soil and above *Rs* decreases with further increase of *T*soil. Above ~27 °C *Rs* stays steady.

Empirical conditional PDFs help to assess changes in the *Rs* distribution given any hydroclimate variable (e.g., *T*soil and/or VWC). The PDF of *Rs* conditioned on one variable (e.g., *T*soil) and two variables (e.g., *T*soil and VWC) can be calculated via equations (2) and (3), respectively (Yue & Rasmussen, 2002):

$$f_{Y|X}(y|x) = [f_X(x) \cap f_Y(y)]/f_X(x) \tag{2}$$

$$f_{Y|X}(y|x,z) = [f_X(x) \cap f_Y(y) \cap f_Z(z)]/[f_X(x) \cap f_Z(z)] \tag{3}$$

where $f_X(x)$, $f_Y(y)$, and $f_Z(z)$ represent the marginal probability distribution function of *T*soil, *Rs*, and VWC, respectively. The mathematical representation of the EP describes the likelihood of *Rs* exceeding a given threshold ($Y > y$) for different values of *T*soil ($X = x_1, x_2, \ldots$) and different values of VWC ($Z = z_1, z_2, \ldots$). To ensure the results are reliable and limited sample size is not affecting the outcomes, we require at least 100 observation points within a *T*soil range of ± 0.5 °C to implement analysis. For purposes of visualizations, we limit the *Rs* range in Figures 5–7 to a max of 5 μmol CO_2/m^2s. Furthermore, we choose the annual mean of *Rs* (1.2 μmol CO_2/m^2s) as the threshold of interest with regards to which we calculate the EP. The EP represents the likelihood that *Rs* exceeds its annual mean, given different hydroclimate conditions. The probability ($\widetilde{P}$) of *Rs* (Y) exceeding a certain threshold (here the annual mean of *Rs*: $\widetilde{y}$) is given by the following integrals:

$$\widetilde{P_x} = \int_{Y > \widetilde{y}} f_{y|x}\, dy \tag{4}$$

$$\widetilde{P_{x,z}} = \int_{Y > \widetilde{y}} f_{y|x,z}\, dy \tag{5}$$

where $\widetilde{P_x}$ and $\widetilde{P_{x,z}}$ represent the shaded area under the PDF curves given by equation (2) in Figures 5 and 7 and equation (3) in Figure 6. The high-frequency data provided through field observations described in section 2.2 enable us to explore if dew presence can describe part of the *Rs* variance observed in the record. We compared night *T*soil surface observations from the data logger with minimum values of the air chamber temperature (*T*cham), which correspond to night temperatures. This seems a reasonable comparison as the chamber is stationed just at a height of ~15 cm above the soil surface. The percent difference (PD) quantifies the difference between these two temperature values.

$$\mathrm{PD} = \left(\frac{1}{x}\sum\left(T\mathrm{cham}_{\mathrm{air\ night}} - T\mathrm{soil}_{\mathrm{surface\ night}}\right)/T\mathrm{soil}_{\mathrm{surface\ night}}\right)*100 \tag{6}$$

where $T\mathrm{cham}_{\mathrm{air\ night}}$, $T\mathrm{soil}_{\mathrm{surface\ night}}$, and x display the minimum value of the night air chamber temperature, night surface soil temperature, and the number of data values, respectively.

3. Results and Discussion

3.1. Temporal Variation of Meteorological Variables and Soil Respiration

Figure 1 shows daily meteorological parameters and *Rs* data. Figure 1a shows low *T*soil during the wet season (November–April) and high *T*soil in the dry season (May–October) and as expected, the temporal variation of VWC follows the precipitation seasonal pattern, that is, Anders and Rockel (2009). It also displays that when VWC is between 0.20 and 0.33 m^3/m^3, *Rs* increases with rainfall, while beyond 0.33 m^3/m^3 when soil becomes saturated (above 0.33 m^3/m^3 dashed line), *Rs* remains insensitive to further rainfall inputs. The study area usually receives most of its precipitation during the wet season followed by a dry season with

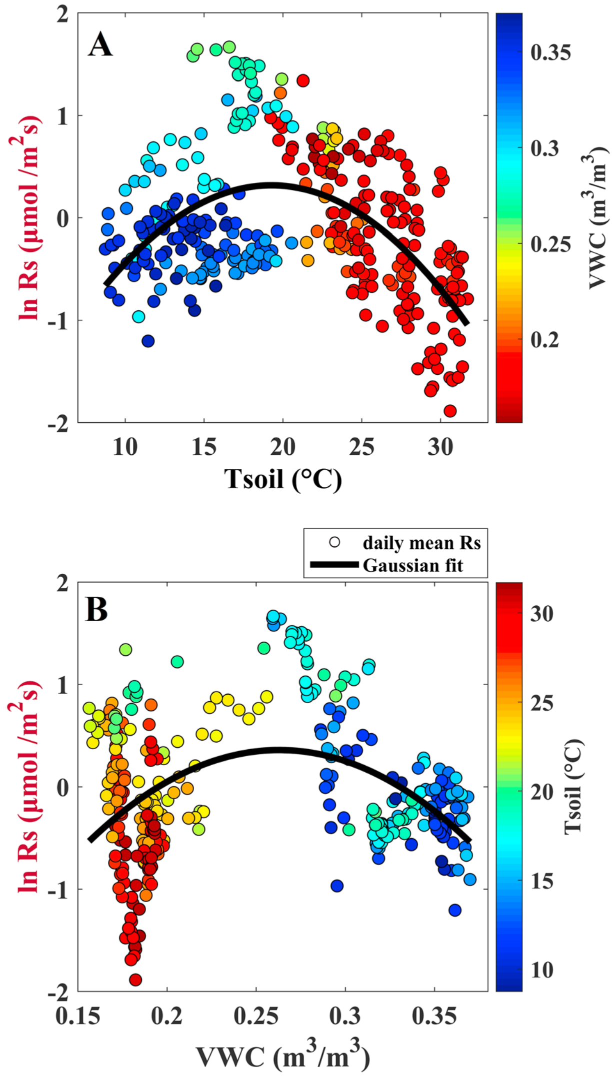

Figure 3. Scatterplot of daily mean values of *Rs*-*T*soil (a) and *Rs*-VWC (b) relationships where the shading of the circles represents the VWC and *T*soil, respectively. *Rs* data are transformed by using natural log function to minimize outliers. Correlation for the *Rs*-*T*soil and *Rs*-VWC relationships is R^2 = 0.28 and R^2 = 0.14, respectively. Gaussian response is fitted to the *Rs*-*T*soil and *Rs*-VWC relationships with the equation: ln (*Rs*) = −0.008821**T*soil^2 + 0.34 * *T*soil −2.96 and ln (*Rs*) = −78.61 * VWC^2 + 41.33 * VWC −5.07, respectively.

relatively low precipitation. The area received, within the study period, ~348 mm of precipitation in total. Figure 1c shows that over the study period, *Rs* varies between −1.01 and 12.37 μmol CO_2/m^2s. These respiration rates are eminently high. However, we found only a few very high measurement points (>10 μmol CO_2/m^2s) and several high values between 6 to 10 μmol CO_2/m^2s; usually *Rs* rates in semiarid areas are measured between ~0.30 and ~2.6 μmol CO_2/m^2s (Oertel et al., 2016; Wang et al., 2014). The results generally imply that *Rs* rises following precipitation events, which is compatible with the results from Deng et al. (2012) and Yan et al. (2014).

3.2. Regression Analysis

Figure 2 depicts the variation in *Rs* and VWC values that are bin averaged within the given step size of 1 °C with respect to *T*soil. VWC plays a significant role in *Rs* and is, therefore, indispensable to be neglected (Qi et al., 2002). Especially in Mediterranean and semiarid ecosystems it needs to be taken into account, where *Rs* is highly sensitive to VWC (Chang et al., 2014; Yan et al., 2014). We demonstrate that *Rs* is limited both when VWC is high and *T*soil is low and vice versa, which is compatible with Reinsch et al. (2017). By examining how *T*soil and VWC affect *Rs*, we indicate that *T*soil values below 14 °C and beyond 27 °C and VWC magnitude below 0.20 m^3/m^3 and beyond 0.32 m^3/m^3 yield limited *Rs*. The limitation of *Rs* at high *T*soil in other ecosystems has been reported by Portner et al. (2010) and Richardson et al. (2012). VWC shows a mirrored sigmoid response function, which is basically a mirrored S form, across the *T*soil range (Schulze, 2000). VWC stays around ~0.33 m^3/m^3 when *T*soil is below ~14 °C, and it decreases gradually below wilting point with increasing *T*soil. At *T*soil above ~23 °C, VWC remains nearly constant by ~0.19 m^3/m^3. High and low VWC diminish the temperature response of *Rs* due to the potential oxygen limitations and metabolic drought stress, respectively (Chang et al., 2014). Other factors such as CO_2 diffusion into pore spaces and CO_2 dissolution in pH water could also limit the temperature response of *Rs* (van Haren et al., 2017).

A similarly Gaussian (bell-shape) pattern in the *Rs* response across the *T*soil ranges is visible, which corroborates with the findings of Carey et al. (2016) and Portner et al. (2010). Figure 2 shows that below ~18 °C, *Rs* increases to nearly ~1.8 μmol CO_2/m^2s and by exceeding ~18 °C, *Rs* decreases to ~1 μmol CO_2/m^2s. Beyond ~27 °C, *Rs* remains nearly unchanged with increasing *T*soil. The latter can be attributed to the fact that biological systems are expected to lower in activity beyond some temperature optima (Schipper et al., 2014). It is not realistic to expect a continuous increase with rising temperature; therefore, the growth must cease and begin to decrease as *T*soil increases above key levels influencing organismal function (Tuomi et al., 2008). Thus, fitting models like the exponential (Q_{10} model), Arrhenius or Lloyd-Taylor equations that do not take into account the declining trend of *Rs* after a metabolic threshold have limited applicability for response dynamics prediction of soil to temperature change (BěHráDek, 1930; Carey et al., 2016). These fitting models generally describe an exponential increase of *Rs* with increasing temperature and can only be used in a narrow temperature range. Previous studies have discussed the inability of these fitting models to represent the response of *Rs* across a wide temperature range, where a decrease of *Rs* takes place.

To describe the relationship between *Rs*-*T*soil and *Rs*-VWC in Figures 3a and 3b, we use a log-quadratic *T*soil (VWC) response function, which is a Gaussian-type model (Carey et al., 2016; Heskel et al., 2016; Lellei-Kovács et al., 2011).

10.1029/2018JG004640

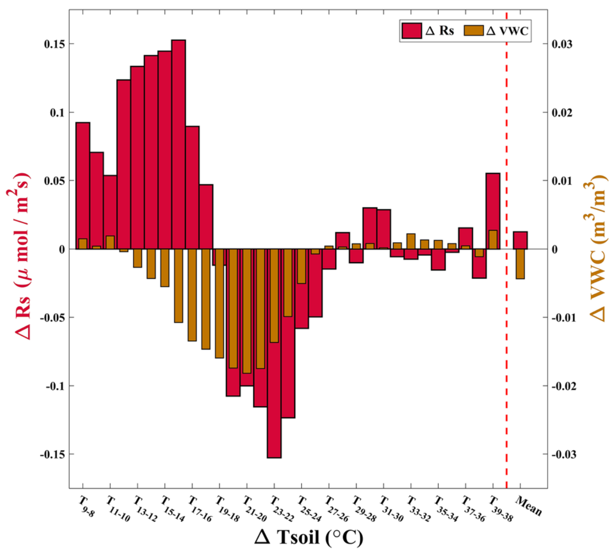

Figure 4. Temperature sensitivity of *Rs* and volumetric water content (VWC). Temperature sensitivity of *Rs* is positive <18 °C ($T_{18\text{-}17}$), negative in between 18 and 27 °C ($T_{27\text{-}26}$) and weak >27 °C. The mean (right side beyond the red dotted line) represents the average of Δ*Rs* and ΔVWC over the entire temperature range. On average Δ*Rs* and ΔVWC display an increase of ~0.013 ± 0.086 (μmol CO_2/m^{2}s) and a decrease of ~ −0.004 ± 0.007 (m^3/m^3) per 1 °C, respectively.

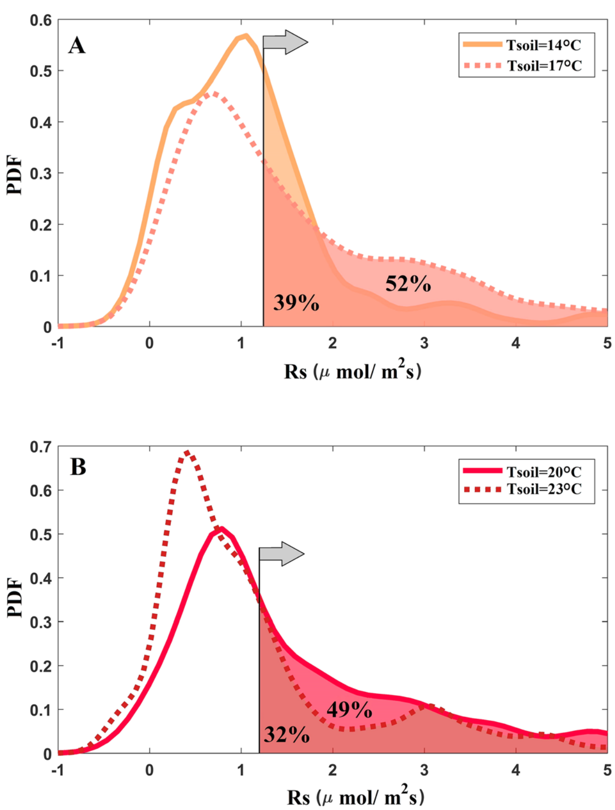

Figure 5. Two panels with conditional probability density functions (PDFs) of *Rs* under four different *T*soil scenarios. The panels show the probability of exceeding annual mean of *Rs* (1.2 μmol CO_2/m^{2}s) given different *T*soil.

$$\ln(Rs) = aX^2 + bX + c \qquad (7)$$

where *Rs* is soil respiration, *X* is either soil temperature (*T*soil) or soil VWC, and *a*, *b*, and *c* are variables to be calibrated. We fit this log-quadratic *T*soil (VWC) response function with daily mean values of *Rs*. In addition, we display in the *z* axis the shading of the circles in the panels (a) and (b) as VWC and *T*soil, respectively. The results are compatible with our findings from Figure 2 where *Rs* is limited at both low *T*soil and high VWC and vice versa.

3.3. Temperature Sensitivity of *Rs* and VWC

Figure 4 shows the temperature sensitivity of *Rs* (Δ*Rs*) and VWC (ΔVWC) per 1 °C change in *T*soil through moving bin averages (equation (1)). Figure 4 reveals that Δ*Rs* is nonlinear across all *T*soil ranges, because it responses to a combination of variability in *T*soil and VWC (Qi et al., 2002). It is also visible that Δ*Rs* is positive at temperatures below ~18 °C ($T_{18\text{-}17}$) and negative at temperatures between ~18 and ~27 °C ($T_{28\text{-}27}$). Above ~27 °C a weak (no significant trend) Δ*Rs* is detectable. We conclude that the positive or negative Δ*Rs* indicates an increase or decrease of *Rs*, respectively. We infer that Δ*Rs* is greatest at low *T*soil and declines as *T*soil increases, which is consistent with the finding of Schipper et al. (2014). Tucker and Reed (2016) also concluded a positive Δ*Rs* at low to moderate *T*soil and a negative Δ*Rs* during summer which is associated with high *T*soil. A number of studies have described the negative Δ*Rs* above a certain *T*soil threshold (Cable et al., 2011; Tucker & Reed, 2016). The reason for the weak Δ*Rs* could be due to the low VWC at high *T*soil or microbial protein denaturation (Carey et al., 2016; Portner et al., 2010). In the ranges of positive, negative, and weak trends, Δ*Rs* is estimated to be ~0.108 ± 0.050, ~−0.075 ± 0.054, and ~0.006 ± 0.024 μmol CO_2/m^{2}s, respectively, although Δ*Rs* over the total range of observed temperature exhibits an increasing trend of ~0.013 ± 0.086 μmol CO_2/m^{2}s per 1 °C.

In Figure 4, ΔVWC shows a nonlinear relationship with *T*soil as well. ΔVWC shows a decreasing response below ~27 °C ($T_{28\text{-}27}$), and above ~27 °C there is no significant trend visible. During negative and no trend ΔVWC, on average ~0.008 ± 0.007 and ~−0.001 ± 0.001 m^3/m^3 is visible, respectively. Overall, ΔVWC decreases by ~0.004 ± 0.007 m^3/m^3 per 1 °C.

3.4. Conditional Probability Analysis

Figure 5 displays the conditional PDF of *Rs* given *T*soil values from 14 to 23 °C with step sizes of 3 °C. In order to show both the increasing and decreasing response of *Rs* to rising *T*soil (as shown in Figure 2), we have selected two ranges where *Rs* observations show opposing responses. The shaded area in both panels show the probability of exceeding the annual mean of *Rs* ($\widetilde{P_x}$; equation (4)) given different *T*soil values. Figure 5a exhibits that when *T*soil reaches 14 °C there is a 39% $\widetilde{P_x}$. One step higher (*T*soil of 17 °C), $\widetilde{P_x}$ increases to 52%. This means that the impact of *T*soil rising from 14 to 17 °C increases $\widetilde{P_x}$ by 33%. Moreover, it is apparent that an increase of *T*soil from 17 to 20 °C demonstrates no significant change in *Rs*, which verifies the tipping point at ~18 °C, as previously mentioned. Therefore, an increase in *T*soil beyond a certain limit yields a smaller $\widetilde{P_x}$. For instance, at *T*soil values of 20 and 23 °C

10.1029/2018JG004640

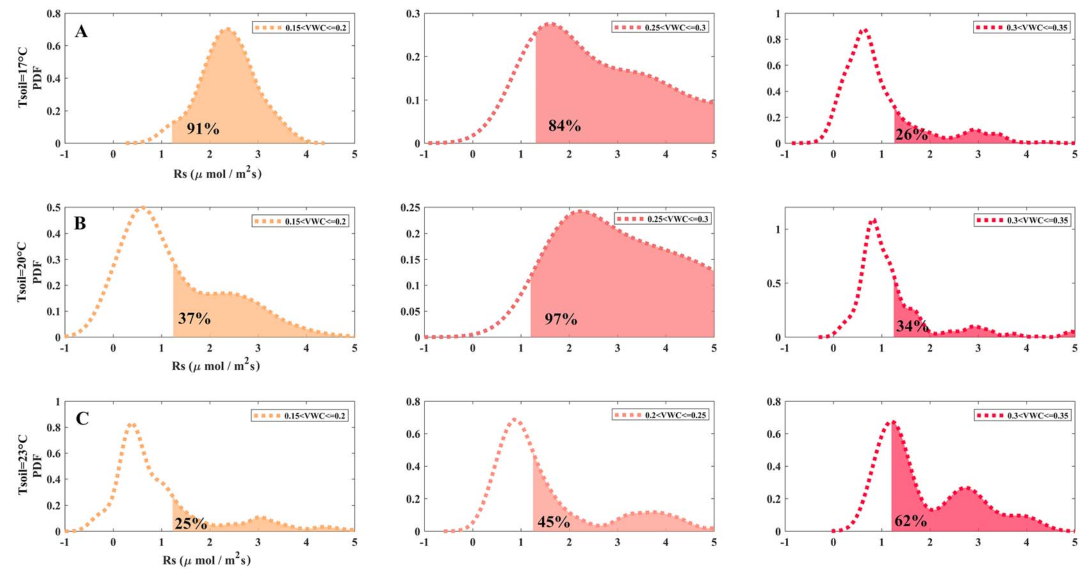

Figure 6. Conditional probability density functions (PDFs) of *Rs* given *T*soil values of 17, 20, and 23 °C and volumetric water content (VWC) values ranging with 0.05-m^3/m^3 step sizes. The shaded area marks the probability of exceeding annual mean of *Rs*. Some VWC ranges are excluded from the panels due to lack of data or insufficient data points at given *T*soil values (see section 2). For instance, we present VWC ranges (0.20–0.25 m^3/m^3) for *T*soil 23 °C (row c, middle) instead of VWC ranges between 0.25 and 0.30 m^3/m^3 due to insufficient observation data under the same *T*soil conditions.

(Figure 5b), $\widetilde{P_x}$ steps down by 35% (from 49% to 32%). Interestingly, the mode (most likely value) of the PDFs decrease as we condition on higher *T*soil values.

In Figure 6 we take VWC into account as an additional covariate affecting *Rs*, to calculate the conditional PDF. In this figure, the shaded area in the panels shows $\widetilde{P_{x,z}}$ (equation (5)) at the given *T*soil values (17, 20, and 23 °C) and VWC values ranging between 0.15 and 0.40 m^3/m^3 with a step size of 0.05 m^3/m^3. Furthermore, some VWC ranges are excluded from the panels in Figure 6 due to either lack of data or insufficient data points (see section 2) at the given *T*soil values. For example, we did not have sufficient observations for VWC ranges between 0.25 and 0.30 m^3/m^3 for *T*soil at 23 °C, and hence, no result is reported. However, we did have sufficient data points for VWC ranges 0.20–0.25 m^3/m^3 under the same *T*soil conditions, and the results are presented in its place (Figure 6c, middle). Row (a) shows that when *T*soil reaches 17 °C, the mode of the *Rs* distribution shifts to lower *Rs* rates, as VWC rises. Therefore, the chance that *Rs* goes beyond the annual mean ($\widetilde{P_{x,z}}$) with rising VWC reduces from 94% to 84% and then to 26%. Row (b) shows that the impact of rising VWC conditioned on *T*soil at 17 °C reduces $\widetilde{P_{x,z}}$ by 71%. This supports our findings that in lower *T*soil values, an increase in VWC corresponds with decreasing *Rs* rates. However, with an increase in *T*soil and VWC this relationship reverses. In row (c), we observe that the mode of *Rs* shifts to higher values, with increasing VWC. Thus, $\widetilde{P_{x,z}}$ increases by 148% (from 25% to 62%). It is worth noting the mode of the *Rs* distribution shifts significantly to lower values with increasing *T*soil, as shown in column 1 (VWC < 0.20 m^3/m^3). $\widetilde{P_{x,z}}$ declines from 91% to 25% with increasing *T*soil. Interestingly, the third column (VWC > 0.30 m^3/m^3) portrays that the mode of *Rs* shifts higher with increasing *T*soil. Consequently, $\widetilde{P_{x,z}}$ increases by a factor of 1.38, from 26% to 62%.

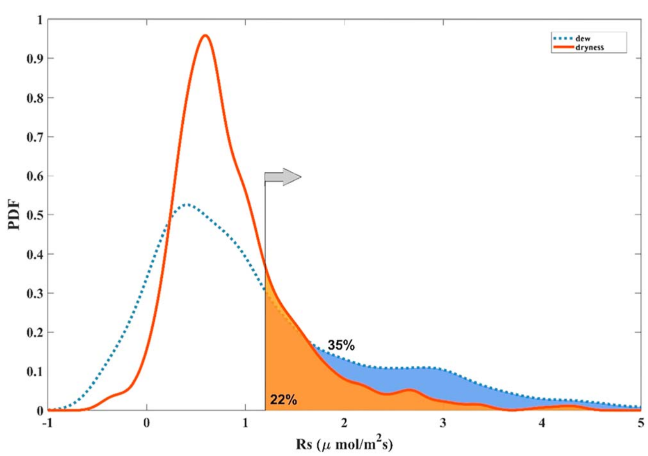

Figure 7. Conditional probability density functions (PDFs) of *Rs* under dryness and dew shows the chance of exceeding annual mean of *Rs*.

3.5. An Overlooked Source of Moisture

Even though no precipitation events occurred during the dry season, we observed random *Rs* increases in various magnitudes and durations, especially from June onward. *Rs* is mainly controlled by *T*soil and VWC, and since *T*soil is sufficiently available, we hypothesize that an overlooked source of moisture other than precipitation is influencing *Rs*. Various mechanisms (e.g., fog, dew, and water vapor adsorption) have been discussed to explain how water, besides precipitation, infiltrates soil's surface layer (Agam & Berliner, 2006; Beysens, 1995; McHugh et al., 2015). Several studies have suggested that dew is an important source of water in drylands, including arid and semiarid areas (Malek et al., 1999; McHugh et al., 2015; Shen et al., 2008). Dew is generally formed when *T*soil surface is lower than or equal to *T*dew, during which water vapor from the air in contact with the cold soil surface condenses in dew (Agam & Berliner, 2006; Beysens, 1995). The resulting condensed water then seeps into the soil and stimulates roots and microbial activity (Escolar et al., 2015).

The PD (equation (6)) of night air *T*cham and night *T*soil surface shows only a ~5% discrepancy. This leads to the conclusion that *T*soil surface matches with the air *T*cham during the night. We, therefore, use the min values of the air chamber temperature to identify time periods where *T*soil surface is lower than dew point temperature (*T*dew) indicating dew formation. Figure 7 displays the PDF of *Rs* conditioned on dryness (*T*soil surface > *T*dew) and dew (*T*soil surface ≤ *T*dew). The shaded area displays $\widetilde{P_x}$ (equation (4)) equal to 22% and 35% given dryness and dew, respectively. This means that the presence of dew causes an increase of $\widetilde{P_x}$ by 60%. Thus, the process of absorption of water vapor into the soil surface has the potential to be a crucial contributor to the carbon cycling in semiarid areas. Our result compatible with previous studies show dew is a main factor besides *T*soil and VWC for assessing *Rs* in dry seasons (Escolar et al., 2015; Jacobson et al., 2015; McHugh et al., 2015; Wang et al., 2014).

4. Conclusion

Soil respiration (*Rs*) is a critical component of the carbon cycle and peculiarly sensitive to climate variability. We use a probabilistic model to describe the change in the entire *Rs* distribution under various hydroclimatic conditions. We analyze and characterize measured high-frequency data of *Rs* on bare soil to enhance our understanding of the temporal *Rs* dynamics. We use subhourly records of *Rs* and other parameters from February 2016 to February 2017 obtained in a semiarid ecosystem in Southern California. *Rs* follows a similar Gaussian pattern with increasing soil temperature (*T*soil). Rate of *Rs* increases below ~18 °C, decreases up to ~27 °C, and shows almost no response beyond ~27 °C, with increasing *T*soil. We use the probabilistic model to assess both the increasing and decreasing response of *Rs* with increasing *T*soil. We have selected two ranges with step sizes of 3 °C where *Rs* show opposing responses. When *T*soil increases from 14 to 17 °C the probability of exceeding annual mean of *Rs* (1.2 μmol CO_2/m^2s) increases by 33%. Furthermore, we show that with increasing *T*soil from 20 to 23 °C the probability of exceeding the annual mean of *Rs* declines by 35%. By considering VWC in conjunction with *T*soil in the probabilistic model, we reveal that increasing VWC at lower temperatures (e.g., 17 °C) decreases the probability of exceeding annual mean of *Rs*. However, this characteristic changes with increasing *T*soil; higher values of *T*soil (e.g., 23 °C) result in an increase in the probability of exceeding annual mean of *Rs*, with rising VWC. Furthermore, we display that during dew the probability of exceeding the annual mean of *Rs* could increase up to 60%. Overall, we show that by using the probabilistic model, we gain information on the entire distribution of the reaction of *Rs* with changing *T*soil and VWC; we assess the impacts of changes in *T*soil and VWC on *Rs*. The proposed model allows detecting changes in the *Rs* distribution due to shifts in hydroclimatic drivers such as *T*soil and VWC. The method is general and can be applied to different applications and variables.

Acknowledgments
This project was partially support by the National Aeronautics and Space Administration (NASA) grant (NNX16AO56G), National Oceanic and Atmospheric Administration (NOAA) grant (NA14OAR4310222), and California Energy Commission grant (500-15-005). Interested readers can access the data used in this study via the website (http://amir.eng.uci.edu/downloads/Data.zip).

References

Agam, N., & Berliner, P. R. (2006). Dew formation and water vapor adsorption in semi-arid environments—A review. *Journal of Arid Environments*, *65*(4), 572–590. https://doi.org/10.1016/j.jaridenv.2005.09.004

Anders, I., & Rockel, B. (2009). The influence of prescribed soil type distribution on the representation of present climate in a regional climate model. *Climate Dynamics*, *33*(2-3), 177–186. https://doi.org/10.1007/s00382-008-0470-y

BěHráDek, J. (1930). Temperature coefficients in biology. *Biological Reviews*, *5*(1), 30–58. https://doi.org/10.1111/j.1469-185X.1930.tb00892.x

Beysens, D. (1995). The formation of dew. *Atmospheric Research*, *39*(1-3), 215–237. https://doi.org/10.1016/0169-8095(95)00015-J

Boone, R. D., Nadelhoffer, K. J., Canary, J. D., & Kaye, J. P. (1998). Roots exert a strong influence on the temperature sensitivity of soil respiration. *Nature*, *396*(6711), 570–572. https://doi.org/10.1038/25119

Bowler, P. (2007). Seasonal marsh habitat restoration and monitoring plan (No. Corps File 9800623).

Cable, J. M., Ogle, K., Lucas, R. W., Huxman, T. E., Loik, M. E., Smith, S. D., et al. (2011). The temperature responses of soil respiration in deserts: A seven desert synthesis. *Biogeochemistry*, *103*(1-3), 71–90. https://doi.org/10.1007/s10533-010-9448-z

Cable, J. M., Ogle, K., Williams, D. G., Weltzin, J. F., & Huxman, T. E. (2008). Soil texture drives responses of soil respiration to precipitation pulses in the Sonoran Desert: Implications for climate change. *Ecosystems*, *11*(6), 961–979. https://doi.org/10.1007/s10021-008-9172-x.
California Resources Agency (2007). San Joaquin Marsh.
Cannone, N., Binelli, G., Worland, M. R., Convey, P., & Guglielmin, M. (2012). CO_2 fluxes among different vegetation types during the growing season in Marguerite Bay (Antarctic Peninsula). *Geoderma*, *189-190*, 595–605. https://doi.org/10.1016/j.geoderma.2012.06.026
Carey, J. C., Tang, J., Templer, P. H., Kroeger, K. D., Crowther, T. W., Burton, A. J., et al. (2016). Temperature response of soil respiration largely unaltered with experimental warming. *Proceedings of the National Academy of Sciences of the United States of America*, *113*(48), 13,797–13,802. https://doi.org/10.1073/pnas.1605365113
Chang, C.-T., Sabaté, S., Sperlich, D., Poblador, S., Sabater, F., & Gracia, C. (2014). Does soil moisture overrule temperature dependency of soil respiration in Mediterranean riparian forests? *Biogeosciences Discussions*, *11*(6), 7991–8022. https://doi.org/10.5194/bgd-11-7991-2014
Cheng, L., AghaKouchak, A., Gilleland, E., & Katz, R. W. (2014). Non-stationary extreme value analysis in a changing climate. *Climatic Change*, *127*(2), 353–369. https://doi.org/10.1007/s10584-014-1254-5
Davidson, E. A., & Janssens, I. A. (2006). Temperature sensitivity of soil carbon decomposition and feedbacks to climate change. *Nature*, *440*(7081), 165–173. https://doi.org/10.1038/nature04514
Deng, Q., Hui, D., Zhang, D., Zhou, G., Liu, J., Liu, S., et al. (2012). Effects of precipitation increase on soil respiration: A three-year field experiment in subtropical forests in China. *PLoS One*, *7*(7), e41493. https://doi.org/10.1371/journal.pone.0041493
Escolar, C., Maestre, F. T., & Rey, A. (2015). Biocrusts modulate warming and rainfall exclusion effects on soil respiration in a semi-arid grassland. *Soil Biology and Biochemistry*, *80*, 9–17. https://doi.org/10.1016/j.soilbio.2014.09.019
Eugster, W., & Merbold, L. (2015). Eddy covariance for quantifying trace gas fluxes from soils. *The Soil*, *1*(1), 187–205. https://doi.org/10.5194/soil-1-187-2015
Evans, S. E., & Wallenstein, M. D. (2012). Soil microbial community response to drying and rewetting stress: Does historical precipitation regime matter? *Biogeochemistry*, *109*(1-3), 101–116. https://doi.org/10.1007/s10533-011-9638-3
Fabianek, T., Menšík, L., & Kulhavý, J. (2015). Influence of different tree densities on CO_2 flux from soil in Norway spruce monoculture. *Beskydy*, *8*(1), 47–53. https://doi.org/10.11118/beskyd201508010047
Giardina, C. P., Litton, C. M., Crow, S. E., & Asner, G. P. (2014). Warming-related increases in soil CO_2 efflux are explained by increased below-ground carbon flux. *Nature Climate Change*, *4*(9), 822–827. https://doi.org/10.1038/nclimate2322
Graf Pannatier, E., Dobbertin, M., Heim, A., Schmitt, M., Thimonier, A., Waldner, P., & Frey, B. (2012). Response of carbon fluxes to the 2003 heat wave and drought in three mature forests in Switzerland. *Biogeochemistry*, *107*(1-3), 295–317. https://doi.org/10.1007/s10533-010-9554-y
Grünzweig, J. M., Hemming, D., Maseyk, K., Lin, T., Rotenberg, E., Raz-Yaseef, N., et al. (2009). Water limitation to soil CO_2 efflux in a pine forest at the semiarid "timberline". *Journal of Geophysical Research*, *114*, G03008. https://doi.org/10.1029/2008JG000874
van Haren, J., Dontsova, K., Barron-Gafford, G. A., Troch, P. A., Chorover, J., Delong, S. B., et al. (2017). CO_2 diffusion into pore spaces limits weathering rate of an experimental basalt landscape. *Geology*, *45*(3), 203–206. https://doi.org/10.1130/G38569.1
Heskel, M. A., O'Sullivan, O. S., Reich, P. B., Tjoelker, M. G., Weerasinghe, L. K., Penillard, A., et al. (2016). Convergence in the temperature response of leaf respiration across biomes and plant functional types. *Proceedings of the National Academy of Sciences of the United States of America*, *113*(14), 3832–3837. https://doi.org/10.1073/pnas.1520282113
Hicks Pries, C. E., Castanha, C., Porras, R. C., & Torn, M. S. (2017). The whole-soil carbon flux in response to warming. *Science*, *355*(6332), 1420–1423. https://doi.org/10.1126/science.aal1319
Hirano, T. (2003). Long-term half-hourly measurement of soil CO_2 concentration and soil respiration in a temperate deciduous forest. *Journal of Geophysical Research*, *108*(D20), 4631. https://doi.org/10.1029/2003JD003766
Huang, J., Ji, M., Xie, Y., Wang, S., He, Y., & Ran, J. (2016). Global semi-arid climate change over last 60 years. *Climate Dynamics*, *46*(3-4), 1131–1150. https://doi.org/10.1007/s00382-015-2636-8
Huning, L. S., & AghaKouchak, A. (2018). Mountain snowpack response to different levels of warming. *Proceedings of the National Academy of Sciences of the United States of America*, *115*(43), 10,932–10,937. https://doi.org/10.1073/pnas.1805953115
Huxman, T. E., Snyder, K. A., Tissue, D., Leffler, A. J., Ogle, K., Pockman, W. T., et al. (2004). Precipitation pulses and carbon fluxes in semiarid and arid ecosystems. *Oecologia*, *141*(2), 254–268. https://doi.org/10.1007/s00442-004-1682-4
Jacobson, K., van Diepeningen, A., Evans, S., Fritts, R., Gemmel, P., Marsho, C., et al. (2015). Non-rainfall moisture activates fungal decomposition of surface litter in the Namib Sand Sea. *PLoS One*, *10*(5), e0126977. https://doi.org/10.1371/journal.pone.0126977
Janssens, I. A., Lankreijer, H., Matteucci, G., Kowalski, A. S., Buchmann, N., Epron, D., et al. (2001). Productivity overshadows temperature in determining soil and ecosystem respiration across European forests. *Global Change Biology*, *7*(3), 269–278. https://doi.org/10.1046/j.1365-2486.2001.00412.x
Jenerette, G. D., Scott, R. L., & Huxman, T. E. (2008). Whole ecosystem metabolic pulses following precipitation events. *Functional Ecology*, *22*(5), 924–930. https://doi.org/10.1111/j.1365-2435.2008.01450.x
Kocárek, M. & Kodešová, R. (2012). Influence of temperature on soil water content measured by ECH2O-TE sensors. *International Agrophysics*, *26*(3), 259–269. https://doi.org/10.2478/v10247-012-0038-2
Kuzyakov, Y., & Gavrichkova, O. (2010). REVIEW: Time lag between photosynthesis and carbon dioxide efflux from soil: A review of mechanisms and controls. *Global Change Biology*, *16*(12), 3386–3406. https://doi.org/10.1111/j.1365-2486.2010.02179.x
Lehmann, J., & Kleber, M. (2015). The contentious nature of soil organic matter. *Nature*. https://doi.org/10.1038/nature16069
Lellei-Kovács, E., Kovács-Láng, E., Botta-Dukát, Z., Kalapos, T., Emmett, B., & Beier, C. (2011). Thresholds and interactive effects of soil moisture on the temperature response of soil respiration. *European Journal of Soil Biology*, *47*(4), 247–255. https://doi.org/10.1016/j.ejsobi.2011.05.004
Liang, N., Teramoto, M., Takagi, M., & Zeng, J. (2017). High-resolution data on the impact of warming on soil CO_2 efflux from an Asian monsoon forest. *Scientific Data*, *4*, 170026. https://doi.org/10.1038/sdata.2017.26
Maier, M., Schack-Kirchner, H., Hildebrand, E. E., & Schindler, D. (2011). Soil CO_2 efflux vs. soil respiration: Implications for flux models. *Agricultural and Forest Meteorology*, *151*(12), 1723–1730. https://doi.org/10.1016/j.agrformet.2011.07.006
Malek, E., McCurdy, G., & Giles, B. (1999). Dew contribution to the annual water balances in semi-arid desert valleys. *Journal of Arid Environments*, *42*(2), 71–80. https://doi.org/10.1006/jare.1999.0506
Mazdiyasni, O., AghaKouchak, A., Davis, S., Madadgar, S., Mehran, A., Ragno, E., et al. (2017). Increasing probability of mortality during Indian heat waves. *Science Advances*, *3*(6), e1700066. https://doi.org/10.1126/sciadv.1700066
McHugh, T. A., Morrissey, E. M., Reed, S. C., Hungate, B. A., & Schwartz, E. (2015). Water from air: An overlooked source of moisture in arid and semiarid regions. *Scientific Reports*, *5*(1). https://doi.org/10.1038/srep13767

Moftakhari, H. R., AghaKouchak, A., Sanders, B. F., & Matthew, R. A. (2017). Cumulative hazard: The case of nuisance flooding. *Earth's Future*, *5*(2), 214–223. https://doi.org/10.1002/2016EF000494

Nuanez, M. (2015). *Quantifying temperature sensitivity of soil respiration across a range of semi-arid biomes*. New Mexico: University of New Mexico.

Oertel, C., Matschullat, J., Zurba, K., Zimmermann, F., & Erasmi, S. (2016). Greenhouse gas emissions from soils—A review. *Chemie der Erde - Geochemistry*, *76*(3), 327–352. https://doi.org/10.1016/j.chemer.2016.04.002

Papalexiou, S. M., AghaKouchak, A., Trenberth, K. E., & Foufoula-Georgiou, E. (2018). Global, regional, and megacity trends in the highest temperature of the year: Diagnostics and evidence for accelerating trends. *Earth's Future*, *6*(1), 71–79. https://doi.org/10.1002/2017EF000709

Phillips, C. L., Bond-Lamberty, B., Desai, A. R., Lavoie, M., Risk, D., Tang, J., et al. (2017). The value of soil respiration measurements for interpreting and modeling terrestrial carbon cycling. *Plant and Soil*, *413*(1-2), 1–25. https://doi.org/10.1007/s11104-016-3084-x

Phillips, C. L., Nickerson, N., Risk, D., & Bond, B. J. (2011). Interpreting diel hysteresis between soil respiration and temperature. *Global Change Biology*, *17*(1), 515–527. https://doi.org/10.1111/j.1365-2486.2010.02250.x

Portner, H., Bugmann, H., & Wolf, A. (2010). Temperature response functions introduce high uncertainty in modelled carbon stocks in cold temperature regimes. *Biogeosciences*, *7*(11), 3669–3684. https://doi.org/10.5194/bg-7-3669-2010

Qi, Y., Xu, M., & Wu, J. (2002). Temperature sensitivity of soil respiration and its effects on ecosystem carbon budget: Nonlinearity begets surprises. *Ecological Modelling*, *153*(1-2), 131–142. https://doi.org/10.1016/S0304-3800(01)00506-3

Raich, J. W., & Schlesinger, W. H. (1992). The global carbon dioxide flux in soil respiration and its relationship to vegetation and climate. *Tellus Series B: Chemical and Physical Meteorology*, *44*(2), 81–99. https://doi.org/10.1034/j.1600-0889.1992.t01-1-00001.x

Reinsch, S., Koller, E., Sowerby, A., de Dato, G., Estiarte, M., Guidolotti, G., et al. (2017). Shrubland primary production and soil respiration diverge along European climate gradient. *Scientific Reports*, *7*(1). https://doi.org/10.1038/srep43952

Rey, A., Pegoraro, E., Oyonarte, C., Were, A., Escribano, P., & Raimundo, J. (2011). Impact of land degradation on soil respiration in a steppe (*Stipa tenacissima* L.) semi-arid ecosystem in the SE of Spain. *Soil Biology and Biochemistry*, *43*(2), 393–403. https://doi.org/10.1016/j.soilbio.2010.11.007

Richardson, J., Chatterjee, A., & Darrel Jenerette, G. (2012). Optimum temperatures for soil respiration along a semi-arid elevation gradient in southern California. *Soil Biology and Biochemistry*, *46*, 89–95. https://doi.org/10.1016/j.soilbio.2011.11.008

Ryan, M. G., & Law, B. E. (2005). Interpreting, measuring, and modeling soil respiration. *Biogeochemistry*, *73*(1), 3–27. https://doi.org/10.1007/s10533-004-5167-7

Scharlemann, J. P., Tanner, E. V., Hiederer, R., & Kapos, V. (2014). Global soil carbon: Understanding and managing the largest terrestrial carbon pool. *Carbon Management*, *5*(1), 81–91. https://doi.org/10.4155/cmt.13.77

Schimel, D. S. (2010). Drylands in the Earth system. *Science*, *327*(5964), 418–419. https://doi.org/10.1126/science.1184946

Schindlbacher, A., Wunderlich, S., Borken, W., Kitzler, B., Zechmeister-Boltenstern, S., & Jandl, R. (2012). Soil respiration under climate change: Prolonged summer drought offsets soil warming effects. *Global Change Biology*, *18*(7), 2270–2279. https://doi.org/10.1111/j.1365-2486.2012.02696.x

Schipper, L. A., Hobbs, J. K., Rutledge, S., & Arcus, V. L. (2014). Thermodynamic theory explains the temperature optima of soil microbial processes and high Q_{10} values at low temperatures. *Global Change Biology*, *20*(11), 3578–Global Change Biology. https://doi.org/10.1111/gcb.12596

Schulze, E.-D. (2000). *Carbon and nitrogen cycling in European forest ecosystems*. Berlin, Heidelberg, New York: Springer. https://doi.org/10.1007/978-3-642-57219-7

Shen, W., Jenerette, G. D., Hui, D., Phillips, R. P., & Ren, H. (2008). Effects of changing precipitation regimes on dryland soil respiration and C pool dynamics at rainfall event, seasonal and interannual scales. *Journal of Geophysical Research*, *113*, G03024. https://doi.org/10.1029/2008JG000685

Song, W., Chen, S., Zhou, Y., Wu, B., Zhu, Y., Lu, Q., & Lin, G. (2015). Contrasting diel hysteresis between soil autotrophic and heterotrophic respiration in a desert ecosystem under different rainfall scenarios. *Scientific Reports*, *5*(1). https://doi.org/10.1038/srep16779

Todd-Brown, K. E. O., Randerson, J. T., Post, W. M., Hoffman, F. M., Tarnocai, C., Schuur, E. A. G., & Allison, S. D. (2013). Causes of variation in soil carbon simulations from CMIP5 Earth system models and comparison with observations. *Biogeosciences*, *10*(3), 1717–1736. https://doi.org/10.5194/bg-10-1717-2013

Tucker, C. L., & Reed, S. C. (2016). Low soil moisture during hot periods drives apparent negative temperature sensitivity of soil respiration in a dryland ecosystem: A multi-model comparison. *Biogeochemistry*, *128*(1-2), 155–169. https://doi.org/10.1007/s10533-016-0200-1

Tuomi, M., Vanhala, P., Karhu, K., Fritze, H., & Liski, J. (2008). Heterotrophic soil respiration–Comparison of different models describing its temperature dependence. *Ecological Modelling*, *211*, 182–190. https://doi.org/10.1016/j.ecolmodel.2007.09.003

U.S. Department of Agriculture Natural Resources Conservation Service. (n.d.). Web soil survey.

van Bemmelen, J. (1891). Ueber die Bestimmungen des Wassers, des Humus, des Schwefels, der in den Colloidalen Silikaten gebunden Kieselsaeuren, des mangans, u.s.w. im Ackerboden. Landwirtschaftliche Versuch Station 279–290.

Walker, W. R. (1989). *Guidelines for designing and evaluating surface irrigation systems, FAO irrigation and drainage paper*. Rome: Food and Agriculture Organization of the United Nations.

Wang, B., Zha, T. S., Jia, X., Wu, B., Zhang, Y. Q., & Qin, S. G. (2014). Soil moisture modifies the response of soil respiration to temperature in a desert shrub ecosystem. *Biogeosciences*, *11*(2), 259–268. https://doi.org/10.5194/bg-11-259-2014

Web Soil Survey [WWW Document]. (n.d.). Retrieved from https://websoilsurvey.sc.egov.usda.gov/App/WebSoilSurvey.aspx (accessed 2.21.18).

Weltzin, J. F., Loik, M. E., Schwinning, S., Williams, D. G., Fay, P. A., Haddad, B. M., Harte, J., et al. (2003). Assessing the response of terrestrial ecosystems to potential changes in precipitation. *Bioscience*, *53*(10), 941. https://doi.org/10.1641/0006-3568(2003)053[0941:ATROTE]2.0.CO;2

Wieder, W. R., Bonan, G. B., & Allison, S. D. (2013). Global soil carbon projections are improved by modelling microbial processes. *Nature Climate Change*, *3*(10), 909–912. https://doi.org/10.1038/nclimate1951

Williams, W. D. (1999). Salinisation: A major threat to water resources in the arid and semi-arid regions of the world. *Lakes & Reservoirs: Research and Management*, *4*(3-4), 85–91. https://doi.org/10.1046/j.1440-1770.1999.00089.x

Yan, L., Chen, S., Xia, J., & Luo, Y. (2014). Precipitation regime shift enhanced the rain pulse effect on soil respiration in a semi-arid steppe. *PLoS One*, *9*(8), e104217. https://doi.org/10.1371/journal.pone.0104217

Yue, S., & Rasmussen, P. (2002). Bivariate frequency analysis: Discussion of some useful concepts in hydrological application. *Hydrological Processes*, *16*(14), 2881–2898. https://doi.org/10.1002/hyp.1185

Zhang, Q., Katul, G. G., Oren, R., Daly, E., Manzoni, S., & Yang, D. (2015). The hysteresis response of soil CO_2 concentration and soil respiration to soil temperature. *Journal of Geophysical Research: Biogeosciences*, *120*, 1605–1618. https://doi.org/10.1002/2015JG003047
Zhong, Q., Wang, K., Lai, Q., Zhang, C., Zheng, L., & Wang, J. (2016). Carbon dioxide fluxes and their environmental control in a reclaimed coastal wetland in the Yangtze Estuary. *Estuaries and Coasts*, *39*(2), 344–362. https://doi.org/10.1007/s12237-015-9997-4